General Disclaimer

One or more of the Following Statements may affect this Document

- This document has been reproduced from the best copy furnished by the organizational source. It is being released in the interest of making available as much information as possible.

- This document may contain data, which exceeds the sheet parameters. It was furnished in this condition by the organizational source and is the best copy available.

- This document may contain tone-on-tone or color graphs, charts and/or pictures, which have been reproduced in black and white.

- This document is paginated as submitted by the original source.

- Portions of this document are not fully legible due to the historical nature of some of the material. However, it is the best reproduction available from the original submission.

Produced by the NASA Center for Aerospace Information (CASI)

(NASA-TM-84996) A RADIO-FREQUENCY ANALYSIS OF PARABOLOIDAL ANTENNAS LOCATED NEAR DIFFRACTING FENCES (NASA) 47 p
HC A03/MF A01 CSCL 20N

N83-33910

Unclas
G3/09 42020

NASA

Technical Memorandum 84996

A RADIO-FREQUENCY ANALYSIS OF PARABOLOIDAL ANTENNAS LOCATED NEAR DIFFRACTING FENCES

R.F. Schmidt

March 1983

National Aeronautics and
Space Administration

Goddard Space Flight Center
Greenbelt, Maryland 20771

TM84996

A RADIO-FREQUENCY ANALYSIS OF PARABOLOIDAL ANTENNAS LOCATED NEAR DIFFRACTING FENCES

R. F. Schmidt

March 1983

GODDARD SPACE FLIGHT CENTER
Greenbelt, Maryland 20771

A RADIO-FREQUENCY ANALYSIS OF PARABOLOIDAL ANTENNAS LOCATED NEAR DIFFRACTING FENCES

R. F. Schmidt
NASA/Goddard Space Flight Center
Greenbelt, Maryland 20771

ABSTRACT

This document applies the cylindrical waves associated with the Sommerfeld solution for a diffracting half-plane in the evaluation of the effects of secondary radiation on the focal-region-fields of paraboloids. A cross-correlation between the computed focal-region-fields and the feed-antenna-fields is then introduced to determine the modified radiation pattern of paraboloidal antennas. The half-plane solution is adapted to estimate the effects of a polygonal fence on 9-meter S-band and 3-meter S-and Ku-band antennas at the Merritt Island, FL Spacecraft Tracking and Data Network Station.

PRECEDING PAGE BLANK NOT FILMED

CONTENTS

PRECEDING PAGE BLANK NOT FILMED

ILLUSTRATIONS

GLOSSARY OF NOTATION

$\overline{E}$, $\overline{H}$	complex-vector electric and magnetic fields
k	wave-number
ψ	phase
ω	weighting factor of linear polarization states
∇	vector operator (grad)
$i \equiv j$	$\sqrt{-1}$
r	distance
ds	differential area
U	a solution of the three-dimensional wave equation
u, v	particular forms of p and q when $\beta = 0$
p, q	arguments of the Fresnel integral dependent on α, β, k, r, and θ
a	generic parameter equal to u, v, p or q
α, β	azimuthal and polar plane-wave angles-of-arrival (in context)
α, β, γ	Eulerian angles for rotation of fences w.r.t. paraboloid (in context)
α_o	paraboloid
F_i	fences
(r, θ, z)	local cylindrical coordinates for fences or half-planes
F(a)	a form of the complex Fresnel integral
G(a)	a compact form of e^{-ia^2} F(a)
sgn	signum or sign switch
$\overline{R}_1$	unit vector antidirectional to plane wave propagation vector
m_i, n_i	weighting factors in plane wave decomposition
$\overline{r}_{HP}$	vector displacement of local origin of half-planes
[A]	orthogonal rotation matrix
$\overline{n}$	unit normal to a surface

$\overline{K}$	electric sheet-current
λ	wavelength
d_f	horn diameter
V	voltage
$\overline{p}$, $\overline{q}$	complex vector polarization states
Ω	solid angle (steradians)
PW	plane wave
CW_i	cylindrical waves
HP	half-planes
SDT	Sommerfeld diffraction theory
POT	physical optics theory
FRF	focal-region field
δ	perturbation
CCA	cross-correlation algorithm
$\langle\overline{P}\rangle$	time average Poynting vector
S	spherical locus
μ	dummy variable (Appendix A)
μ_o	permeability of free space (henry/meter)
ϵ_o	permittivity of free space (farad/meter)
Z_o	characteristic impedance of free space (ohms)

A RADIO-FREQUENCY ANALYSIS OF PARABOLOIDAL ANTENNAS LOCATED NEAR DIFFRACTING FENCES

INTRODUCTION

This document is an attempt at estimating the effects of proximate diffracting fences on the performance of paraboloidal antennas at the Merritt Island, FL Spacecraft Tracking and Data Network Station. Both 9-meter S-band and 3-meter S-and Ku-band installations are of concern. Mathematical simulation of the paraboloids and the diffracting fences affords a means of assessing the effects as a function of antenna and fence parameters. High-speed digital computers may be used to extract quantitative information from an analysis based on the vector Kirchhoff-Kottler physical optics theory for continuous surfaces and the Sommerfeld diffraction theory for half-planes.

A plane-wave which is incident on a paraboloidal antenna induces an electromagnetic sheet-current on the latter. From this a highly satisfactory computation of the focal-region fields, wavefronts, and time-average Poynting vectors can be made. The assumed primary wave incident on the paraboloid may also illuminate diffracting fences which act as secondary sources. Each fence will radiate a cylindrical wave exhibiting, in general, a linear phase gradient, and a non-trivial field-intensity distribution. If phase is preserved in a mathematical simulation, and all polarization components are included, the total perturbation of the sheet-current on the paraboloid may be calculated and, subsequently, a new set of focal-region fields, wavefronts, and time-average Poynting vectors may be determined.

The far-field radiation pattern of a paraboloid, influenced by one or more diffraction fences, may in principal be found from a knowledge of the focal-region fields and feed-antenna fields over some surface of convenience. A sphere centered on the focal-point of the paraboloid, with radius equal to the far-field distance of a feed horn, is satisfactory for this purpose. A cross-correlation of the focal-region and feed antenna fields, by means of an algorithm

that is responsive to the spatial (vector) and temporal (complex-phase) character of the problem leads to a single voltage for every angle of arrival of an assumed plane-wave. In this manner, the far-field or transmission radiation pattern evolves, from an analysis which is predicated entirely on reception arguments, in the presence of diffracting fences.

PLANE-WAVE SOURCES

Two orthogonal plane-wave sources are admitted in the simulation. See Ref. 1, p. 578.

E – polarization

$$\bar{E} = (-\cos\alpha \sin\beta, -\sin\alpha\sin\beta, \cos\beta)\, e^{-ikS} \qquad (1)$$

$$\bar{H} = (-\sin\alpha, \cos\alpha, 0)\, e^{-ikS} \qquad (2)$$

H – polarization

$$\bar{E} = (\sin\alpha, -\cos\alpha, 0)\, e^{-ikS} \qquad (3)$$

$$\bar{H} = (-\cos\alpha\sin\beta, -\sin\alpha\sin\beta, \cos\beta)\, e^{-ikS} \qquad (4)$$

The phase factor of the plane waves is

$$e^{-ikS} = e^{-ik\,(x\,\cos\alpha\,\cos\beta + y\,\sin\alpha\,\cos\beta + z\,\sin\beta)} \quad . \qquad (5)$$

Angles (α, β) and coordinates (x, y, z), above, were originally in a local context for a half-plane analysis as presented by Born and Wolf, but are now utilized in a global context (GSFC coordinates) for the incident plane wave of the simulation. A given point (x, y, z) on the paraboloid will appear as (x″, y″, z″) at the origin of a rotated and translated diffraction fence. Similarly, angles (α'', β'') will emerge as the local angles of arrival at such a fence. See Fig. 1. It can be seen that (α) is an azimuthal variation in the equatorial (x, y) plane, and (β) is a polar variation emanating from the (x, y) plane.

Any degree of polarization ellipticity, orientation, and rotation sense of the polarized state is available via either (1) and (3) or (2) and (4). It may be more direct to combine two counter-rotating circular states, in any given instance, since the relative phase of the circular states and inclination angle of the polarization ellipse are simply related,

$$\psi_r = 2\psi_i \quad , \qquad (6)$$

the axial ratio of the ellipse derives from the relative weights,

$$AR = (\omega_1 + \omega_2)/(\omega_1 - \omega_2) \quad , \qquad (7)$$

and the rotation sense of the field vector is determined by the larger of (ω_1) and (ω_2).

ORIGINAL PAGE IS
OF POOR QUALITY

SCATTERING FORMULATION (PARABOLOID)

An amended form of the complex-vector Kirchhoff-Kottler formulation (physical optics) suffices to compute the focal region fields, wavefronts, and time-average Poynting vectors of the paraboloid. It is a variation of the Stratton-Chu formula. See Ref. 2, p. 460; Ref. 3, p. 158; Ref. 4, p. 4; Ref. 5, p. 35.

$$\bar{E}(x, y, z) = \frac{1}{j\omega\epsilon}\frac{1}{4\pi}\int_{S_1}[(\bar{n} \times \bar{H}_1) \cdot \nabla]\nabla\psi ds - j\omega\mu\frac{1}{4\pi}\int_{S_1}(\bar{n} \times \bar{H}_1)\,\psi ds \,, \quad (8)$$

$$\bar{H}(x, y, z) = -\frac{1}{4\pi}\int_{S_1}(\bar{n} \times \bar{H}_1) \times \nabla\psi \, ds \quad , \quad (9)$$

$$\psi = e^{jkr}/r \quad , \quad (10)$$

where

$$\nabla\psi = +(jk - \frac{1}{r})\,\psi\,\hat{1}_r \quad . \quad (11)$$

The phase of the Green's function (10) is seen to be consistent with the plane-wave formulation of Born and Wolf, given previously.

ORIGINAL PAGE IS
OF POOR QUALITY

SCATTERING FORMULATION (HALF-PLANE)

The total fields, in local coordinates, for three-dimensional diffraction of a plane wave by a half-plane are given in Ref. 1, p. 579, in the Gaussian system of units as (E-plane polarization)

$$E_x = -H_y \sin\beta \tag{12}$$

$$E_y = H_x \sin\beta \tag{13}$$

$$E_z = \frac{e^{-\pi i/4}}{\sqrt{\pi}} \cos\beta\, e^{ik(r\cos\beta - z\sin\beta)} \left[G(p) - G(q)\right] \tag{14}$$

$$H_x = \frac{-e^{-\pi i/4}}{\sqrt{\pi}} e^{ik(r\cos\beta - z\sin\beta)} \left\{\sin\alpha[G(p) + G(q)] + i\sqrt{\frac{2}{kr\cos\beta}}\, \sin\alpha/2\, \cos\theta/2\right\} \tag{15}$$

$$H_y = \frac{e^{-\pi i/4}}{\sqrt{\pi}} e^{ik(r\cos\beta - z\sin\beta)} \left\{\cos\alpha[G(p) - G(q)] - i\sqrt{\frac{2}{kr\cos\beta}}\, \sin\alpha/2\, \cos\theta/2\right\} \tag{16}$$

$$H_z \equiv 0 \tag{17}$$

As mentioned previously, (x, y, z) above will be redesignated (x″, y″, z″) due to certain correspondences, translations, and rotations among the Cartesian coordinate systems used hereir

The companion expressions to (12) through (17) for the H-plane polarization case are not given explicitly in Ref. 1. It happens that the E-plane polarization case was developed by means of two auxilliary equations,

$$\overline{E} = \left(\frac{-i\sin\beta}{k}\frac{\partial U}{\partial x}, \frac{-i\sin\beta}{k}\frac{\partial U}{\partial y}, \cos^2\beta U\right) \tag{18}$$

and

$$\overline{H} = \left(\frac{-i}{k}\frac{\partial U}{\partial y}, \frac{i}{k}\frac{\partial U}{\partial x}, 0\right) . \tag{19}$$

ORIGINAL PAGE IS
OF POOR QUALITY

The H-plane polarization case may, therefore, be developed using two other auxilliary equations. See Ref. 1. p. 579.

$$\overline{E} = \left(\frac{i}{k} \frac{\partial U}{\partial y} , \frac{-i}{k} \frac{\partial U}{\partial x} , 0 \right) \tag{20}$$

and

$$\overline{H} = \left(\frac{-i \sin \beta}{k} \frac{\partial U}{\partial x} , \frac{-i \sin \beta}{k} \frac{\partial U}{\partial y} , \cos^2 \beta \, U \right) . \tag{21}$$

Details of the derivation may be found in Appendix A of this document. The results are given below, also in the Gaussian system of units, as

(H-plane polarization)

$$E_x = \frac{e^{-\pi i/4} \, e^{ik(r \cos \beta - z \sin \beta)}}{\sqrt{\pi}} \left\{ \sin\alpha[G(p) - G(q)] \oplus i \sqrt{\frac{2}{kr \cos \beta}} \cos \frac{\alpha}{2} \sin \frac{\theta}{2} \right\} \tag{22}$$

$$E_y = \frac{-e^{-\pi i/4} \, e^{ik(r \cos \beta - z \sin \beta)}}{\sqrt{\pi}} \left\{ \cos\alpha[G(p) + G(q)] \oplus i \sqrt{\frac{2}{kr \cos \beta}} \cos \frac{\alpha}{2} \cos \frac{\theta}{2} \right\} \tag{23}$$

$$E_z \equiv 0 \tag{24}$$

$$H_x = E_y \sin \beta \tag{25}$$

$$H_y = -E_x \sin \beta \tag{26}$$

$$H_z = \frac{e^{-\pi i/4} \, e^{ik(r \cos \beta - z \sin \beta)}}{\sqrt{\pi}} [G(p) + G(q)] . \tag{27}$$

Note:

Present derivation (+ i) in equation (22), (+ i) in equation (23).

Ref. 1, 2nd Ed. (- i) in equation (22), (- i) in equation (23).

Ref. 1, 6th Ed. (- i) in equation (22), (+ i) in equation (23).

ORIGINAL PAGE IS
OF POOR QUALITY

The evaluation of G(p) and G(q) presents alternatives. Assume that

$$\beta \leq \pi/2 \tag{24}$$

and

$$\alpha \leq \pi \quad , \tag{25}$$

See Fig. 2, where the diffracting half-plane is bounded by the ±z axis and lies in the (+x) part of the xz-plane. It can be seen that

$$p > 0 \mid_{\theta > \pi + \alpha} \quad , \tag{26}$$

and

$$q > 0 \mid_{\theta > \pi - \alpha} \quad , \tag{27}$$

from an inspection of equations (2A). That is, $p > 0$ in the shadow region (SR) and $q < 0$ in the reflection region (RR).

It can also be seen that the condition for asymptotic evaluation,

$$kr >> 1 \quad , \tag{28}$$

given in Ref. 1, p. 572 for the two-dimensional diffraction of a plane wave by a half-plane, becomes

$$kr \cos \beta >> 1 \tag{29}$$

for the present three-dimensional case. Further, (p) and (q) may vanish under same conditions:

$$p = 0 \mid_{\theta = \pi + \alpha} \tag{30}$$

and

$$q = 0 \mid_{\theta = \pi - \alpha} \quad ,$$

at the shadow and reflection boundaries, respectively, even for large (kr cos β). This indicates that the requirement on (a) for asymptotic evaluation implies

$$p >> 1 \ , \ q >> 1 \tag{31}$$

ORIGINAL PAGE IS
OF POOR QUALITY

From Ref. 1, p. 569,

$$G(a) = e^{-ia^2} F(a) \tag{30}$$

and parameter (a) may be zero, positive, or negative. Here,

$$F(a) = \int_a^{\infty} e^{i\mu^2} d\mu \quad . \tag{31}$$

The development of Ref. 1, p. 572 pertaining to the evaluation of G(a) for negative (a) is not explicit for small values of (a). Appendix B of this document gives the details of a development leading to a general formula,

$$G(a) = e^{-ia^2} \left[\sqrt{\pi}\, e^{\pi i/4}\, U(-a) + \mathrm{sgn}(a) \int_{|a|}^{\infty} e^{i\mu^2} \, d\mu \right] \quad , \tag{32), (7-B}$$

where

$$U(x) \equiv \begin{array}{l} 1 \mid x > 0 \\ 0 \mid x \leqslant 0 \end{array} \tag{33}$$

and

$$\mathrm{sgn}\,(x) = \begin{array}{l} +1 \mid x \geqslant 0 \\ -1 \mid x < 0 \end{array} \tag{34}$$

For large values of (a), equation (32) above reduces to

$$G(a) = \sqrt{\pi}\, e^{\pi i/4}\, e^{-ia^2}\, U(-a) + \mathrm{sgn}(a) \left[\frac{i}{2|a|} + 0 \left(\frac{1}{|a|^3} \right) \right] \quad , \tag{35}$$

which agrees with Ref. 1, excepting a typographical error; (e^{-ia}) should read (e^{-ia^2}), equation (32), page 572.

See Appendix C for a conversion of the Ref. 1 equations, above, to the rationalized MKS system of units.

ORIGINAL PAGE IS
OF POOR QUALITY

COORDINATE SYSTEMS

A convenient means for computing the sheet-current induced on the paraboloidal reflector by the diffracting half-planes or fences is to retain the local coordinate conventions of Born and Wolf, Ref. 1, pp. 556-580. Figure 3 illustrates a reference coordinate system (x, y, z) of the overall problem and the local coordinate system (x′, y′, z′) of a half-plane shown translated from 0 to 0′. It can be seen that a correspondence exists between the two systems prior to translation of origin.

$$(x, y, z) \rightarrow (-x', z', y') \quad . \tag{36}$$

The Cartesian components of vector ($\bar{r}'$) from 0′ to a point on the paraboloidal reflector (γ) may be specified in the (x, y, z) coordinate system using

$$\bar{r}' = \bar{r} - \bar{r}_{HP} = (x, y, z) \tag{37}$$

and rewritten as

$$\bar{r}' = (x', y', z') \tag{38}$$

using the correspondence, (36).

Prior to rotation of the half-plane, the Born and Wolf local cylindrical coordinates (r', θ', z') are then found from

$$x' = r' \cos\theta' \tag{39}$$

or

$$y' = r' \sin\theta' \tag{40}$$

and

$$(r')^2 = |\bar{r}'|^2 = (x')^2 + (y')^2 \quad . \tag{41}$$

ORIGINAL PAGE IS
OF POOR QUALITY

Rotation of the half-plane results in a re-designation of the local coordinate frame as (x″, y″, z″) with origin (0″) at (0′) as shown in Fig. 4. The Cartesian components of vector ($\bar{r}'$) are now different from those of ($\bar{r}''$). The latter are found using

$$(x'', y'', z'') = [A]\ (x', y', z') \tag{42}$$

where

$$[A] = \begin{bmatrix} (\cos\gamma\cos\alpha - \cos\beta\sin\alpha\sin\gamma) & (\cos\gamma\sin\alpha + \cos\beta\cos\alpha\sin\gamma) & (\sin\gamma\ \sin\beta) \\ (-\sin\gamma\cos\alpha - \cos\beta\sin\alpha\cos\gamma) & (-\sin\gamma\sin\alpha + \cos\beta\cos\alpha\cos\gamma) & (\cos\gamma\ \sin\beta) \\ (\sin\beta\ \sin\alpha) & (-\sin\beta\ \cos\alpha) & (\cos\beta) \end{bmatrix}. \tag{43}$$

See Ref. 6, p. 107 for a discussion of Eulerian angles.

The frame (x″, y″, z″) is visualized as rotating with respect to the frame (x′, y′, z′), and requires the rewriting of (39) (40) and (41) in double-prime notation to obtain the Born and Wolf local cylindrical coordinates (r″, θ'', z″). Once the latter are obtained, it is convenient to drop the double-prime notation and enter the Born and Wolf equations with the derived values.

POLYGONAL FENCES

Additional complexity arises when the half-plane formulation is applied repeatedly to mathematically simulate a polygonal fence such as the one illustrated in Fig. 5. Also see flow charts, Figs. 6 and 7. The procedure is justified by the parameters of the present problem and the inherent behavior of the half-plane formulation when $kr \gg 1$. Only S- and Ku-band frequencies are to be introduced into the present calculations, and the fence height and length for each polygonal element exceed 8-feet. Under these conditions a segment of a cylindrical wave is associated with each segment of the fence. Ref. 1, p. 572. Also see Fig. 1 of this document. Points $(\bar{r}', \bar{r}'')$ which either exceed the cylindrical bounds of a finite cylindrical wave, or imply intersection with paraboloid (γ_0), are excluded from consideration.

Assuming that a single plane-wave illuminates the paraboloid directly, together with the several elements of a polygonal fence, it can be seen that a distinct set of input parameters must be associated with each element of the fence. The local plane wave angles-of-arrival (α, β), the local Eulerian angles (α, β, γ), and the displacement vectors $(\bar{r}_{HP})$ are required.

A direct method for finding the set of plane-wave angles-of-arrival is to proceed on the assumption that the fence geometry, in relation to the paraboloid, has been established. Selection of a single pair of values (α, β), for purposes of illuminating the paraboloid, then fixes all of the local angles of arrival for the half-planes. If a unit vector with Cartesian components in the (x, y, z) reference frame is chosen co-linear, but antidirectional with respect to propagation vector of the plane-wave so that

$$\bar{R}_1 = (x, y, z) = (\cos\alpha \cos\beta, \sin\alpha \cos\beta, \sin\beta) \quad , \qquad (44)$$

the wave angles of arrival are obtainable by combining the correspondence (36) and the rotation (42). The translation (37) may be ignored here since only angles are of concern. In each instance the Eulerian angles of the rotation matrix are known and a vector (x'', y'', z'') is the output. The local (α, β) for each half-plane is then found by solving a system of equations

ORIGINAL PAGE IS
OF POOR QUALITY

similar to (44) of the present document. Note that $\bar{R}_1$ is different between Fig. 2 and Fig. 3 due to the preservation of local (α, β) and [A] not equal to the identity matrix.

Assume that selection of the (α, β) pair taken with respect to the (x, y, z) frame leads to an incident linearly-polarized magnetic field whose vector components, without regard to phase, are

$$\bar{H} = (H_x, H_y, H_z) \quad . \quad (45)$$

via either equation (2) or equation (4). This field must now be decomposed into an $\bar{E}_{POL}$ and $\bar{H}_{POL}$ field, so that, in general, the magnetic fields scattered by each half-plane may be evaluated via equations (19) and (21) for E-plane and H-plane polarizations, respectively. It follows, using (2) and (4), that the field of (45) may be written in local coordinates as

$$(H_x'', H_y'', H_z'') = m_1(-\sin\alpha, \cos\alpha, 0) + n_1(-\cos\alpha \sin\beta, -\sin\alpha \sin\beta, \cos\beta) \quad , \quad (46)$$

where (m_1) and (n_1) are the unknown weights of two orthogonal, cophased plane-waves incident on the half-plane. The angles (α, β) of (46) are now the local angles of arrival, computed previously, so that (46) is a system of three equations in two unknowns. This leads to

$$(H_x'', H_y'', H_z'') = m_1 \bar{H}_{E\text{-}POL.} + n_1 \bar{H}_{H\text{-}POL.} \quad . \quad (47)$$

In the event that an elliptically-polarized phane wave is incident on the paraboloid (γ_o) and the half-planes or fences, a second and similar resolution of the type discussed is required. This leads to an illumination of the form

$$\bar{H}_{TOT} = (m_1 \bar{H}_{E\text{-}POL} + n_1 \bar{H}_{H\text{-}POL}) e^{j\psi_1} + (m_2 \bar{H}_{E\text{-}POL} + n_2 \bar{H}_{H\text{-}POL}) e^{j\psi_2} \quad , (48)$$

where (m_1, n_1, m_2, n_2) are scalar weighting factors and (ψ_1, ψ_2) are scalar phase-constants affecting rotation sense, axial ratio, and inclination angle of a preferred elliptical state.

A correction remains to be made concerning phase. The solutions of the half-plane problem were originally obtained using a phase factor given by (5), with the origin of coordinates

ORIGINAL PAGE IS
OF POOR QUALITY

on the diffracting edge. Since the incident plane-wave has been referenced to the origin (0) of the (x, y, z) frame the phase at the various origins (0″) is given by a factor

$$F = e^{-ik\bar{R}_1 \cdot \bar{r}_{HP}} \tag{49}$$

which now must be applied to the scattered fields of the half-planes or fences. The $\bar{r}_{HP}$ are, in general, distinct when several fences are encountered, but there is only one value of $\bar{R}_1$ (antidirectional to the propagation direction of the incident plane wave). See Fig. 5 which depicts a polygonal fence.

The total fields associated with each half-plane or fence are evaluated in a local context for every point on the paraboloidal reflector (γ_0) and must be converted to the global context of the problem. Since the magnetic field components are expressed in the (x″, y″, z″) system of coordinates,

$$(H_x', H_y', H_z') = [A]^{-1} (H_x'', H_y'', H_z'') \tag{50}$$

Once (H_x', H_y', H_z') have been determined, the correspondence of (36) is used in the inverse sense.

$$(H_x', H_y', H_z') \rightarrow (-H_x, H_z, H_y) \tag{51}$$

The translations ($\bar{r}_{HP}$) are irrelevant since translation does not affect projections between two non-congruent coordinate frames. In the preceding $[A]^{-1}$ is, in general, distinct for the half-planes or fences since the Eulerian angles (α, β, γ) are distinct.

Once the total magnetic fields associated with the diffracting fences have been computed and the geometric optics field has been subtracted for each fence, a superposition of sheet currents may be visualized. That is,

$$\bar{K}_{TOT} = \underbrace{2\bar{n} \times \bar{H}_i}_{\text{(primary induction)}} + \underbrace{2\bar{n} \times (\bar{H}s_1 + \bar{H}s_2 + \bar{H}s_3 + \ldots \bar{H}s_i)}_{\text{(secondary induction)}} \tag{52}$$

for (i) half-planes or fences. The focal region fields may then be computed using equations (8)

through (11) of this document in conjunction with the incident magnetic fields of (52). See Figs. 6 and 7 for a flow chart of the preceding operations, and Appendix D for a discussion relating to the total field.

ORIGINAL PAGE IS
OF POOR QUALITY

CROSS-CORRELATION (FOCAL-REGION FIELDS AND FEED FUNCTION)

An algorithm is now written to express the received voltage as a cross-correlation between a completely polarized focal-region and a feed function. Such a voltage represents one point of an aperture-antenna radiation pattern. The cross-correlation is effected on a spherical locus, as shown in Fig. 8, for convenience. Its radius is the far-field distance of the feed horn,

$$Rs = \frac{2d_f^2}{\lambda} \quad , \qquad (53)$$

The algorithm derives directly from the fact that the induced voltage which results from the interaction of two elliptical states is given by

$$V_{OC} = \bar{q}^* \cdot \bar{p} \quad , \qquad (54)$$

where $\bar{q}^*$ is the complex-conjugate of the received field and $\bar{p}$ represents a linear receiving antenna. See Ref. 8, p. 105, Ref. 9, p. 184. When $\bar{p}$ and $\bar{q}$ are both unit complex-vectors, an expression for polarization efficiency may be written as

$$\eta_{POL} = | \bar{p} \cdot \bar{q}^* |^2 \quad , \qquad (55)$$

In the subject cross-correlation for receiving apertures equation (54) becomes

$$V_{OC} = \iint_{\Omega} \bar{E}_R^* \cdot \bar{E}_f \; d\Omega \quad . \qquad (56)$$

Here $(\bar{E}_R)$ is a complex-vector focal-region field and $(\bar{E}_f)$ is characterized by the feed function. In the present context the received field may be regarded as having the dimensions (volts/meter^1), and the feed function acts as an effective height (meter^1) per unit solid angle (Ω). The differential solid angle ($d\Omega$) may be formally associated with area (dS) on the spherical locus (S) via

$$d\Omega = \frac{\bar{r} \cdot \bar{n}_1}{r^3} \; dS \qquad (57)$$

ORIGINAL PAGE IS
OF POOR QUALITY

where

$$|\bar{r}| \equiv Rs \tag{58}$$

and the unit normal ($\bar{n}_1$) is that of a sphere. See Ref. 10, p. 290. It is noted that ($\bar{E}_R$) and ($\bar{E}_f$) are, in general, not unit quantities in (56) and only relative voltage is required for a radiation pattern.

The magnetic counterpart to (56) may therefore be written as a proportionality:

$$V_{OC} \propto \iint_{\Omega} \bar{H}_R^* \cdot \bar{H}_f \, d\Omega \quad . \tag{59}$$

The magnetic field ($\bar{H}_R$) incident on the locus (S) is obtained from equation (9). The term ($\bar{H}_f$) depends on the feed function selected for the calculation. It may be as simple as

$$\bar{H}_f = \frac{A \cos^N \Theta}{\rho} \bar{h}_i \quad , \tag{60}$$

where

$$\bar{h}_i = \frac{\bar{\rho} \times \bar{v}}{|\bar{\rho} \times \bar{v}|} \quad . \tag{61}$$

Here (A) is a scalar amplitude, (N) is a directivity factor, Θ is a polar angle taken with respec to the feed horn axis, ($\bar{v}$) is a polarization moment, and

$$|\bar{\rho}| \equiv Rs \quad . \tag{62}$$

Many other representations are possible: rigorously derived expressions for feed horns and open waveguides, numerical data, etc.

Returning to Fig. 8(a), it appears that a rotationally symmetric situation exists when the primary or incident plane-wave is axially directed ($\alpha = \pi/2$, $\beta = \pi/2$). This is somewhat illusory since the rule for current induction

$$\bar{K} = 2\bar{n} \times \bar{H}_i \tag{63}$$

converts the axial symmetry associated with the paraboloid to uniplanar symmetry. This uniplanar symmetry persists for ($\alpha < \pi/2$, $\beta = \pi/2$), or paraxial wave arrival, although the received fields ($\overline{E}_R$) are now displaced with respect to the feed function ($\overline{E}_f$), as suggested by Fig. 8(b). Introduction of diffraction fences, Fig. 8(c), will leave the calculation entirely without symmetry.

CONCLUSION

This document constitutes the first or analytical phase of an attempt to estimate the effects of proximate diffracting fences on the performance of paraboloidal antennas at the Merritt Island, FL Spacecraft Tracking and Data Network Station. The second and third phases are the writing and verification of a computer program which incorporates the theory presented herein, and the actual generation of numerical data for assumed antenna and geometrical parameters. Introduction of fence mesh details in a higher level analysis, attendant program modification, and subsequent numerical calculations, constitute possible additional phases.

An appreciation of the antenna environment may be formed from Fig. 9, which shows the Kennedy Space Center Layout (KSC). The effects of the diffraction fences are seen to be a function of antenna pointing angle, elevation, range, and frequency. A photograph showing the 30′ (9-meter) USB Antenna, No. 2, is included as Fig. 10 and should be compared to the abstraction originally presented as Fig. 1. It appears, from the large number of parameters, the repeated appearance of integrals in the present formulations, the relatively high frequencies of operation (S- and Ku-bands) and the electrical size of the antennas (3-meter, 9-meter), that a highly organized approach to the overall problem is imperative. Accordingly the programming is proceeding with careful monitoring of computer core and cpu requirements. Option switches are being incorporated as suggested by Figs. 6 and 7. Initial computations will be restricted to linear polarization and single-fence configurations to obtain program verification although the program will be written to accommodate arbitrary angle of primary wave arrival, elliptical polarization states for the received fields and the feed horn characteristics, and polygonal fences with elevation contours included.

ORIGINAL PAGE IS
OF POOR QUALITY

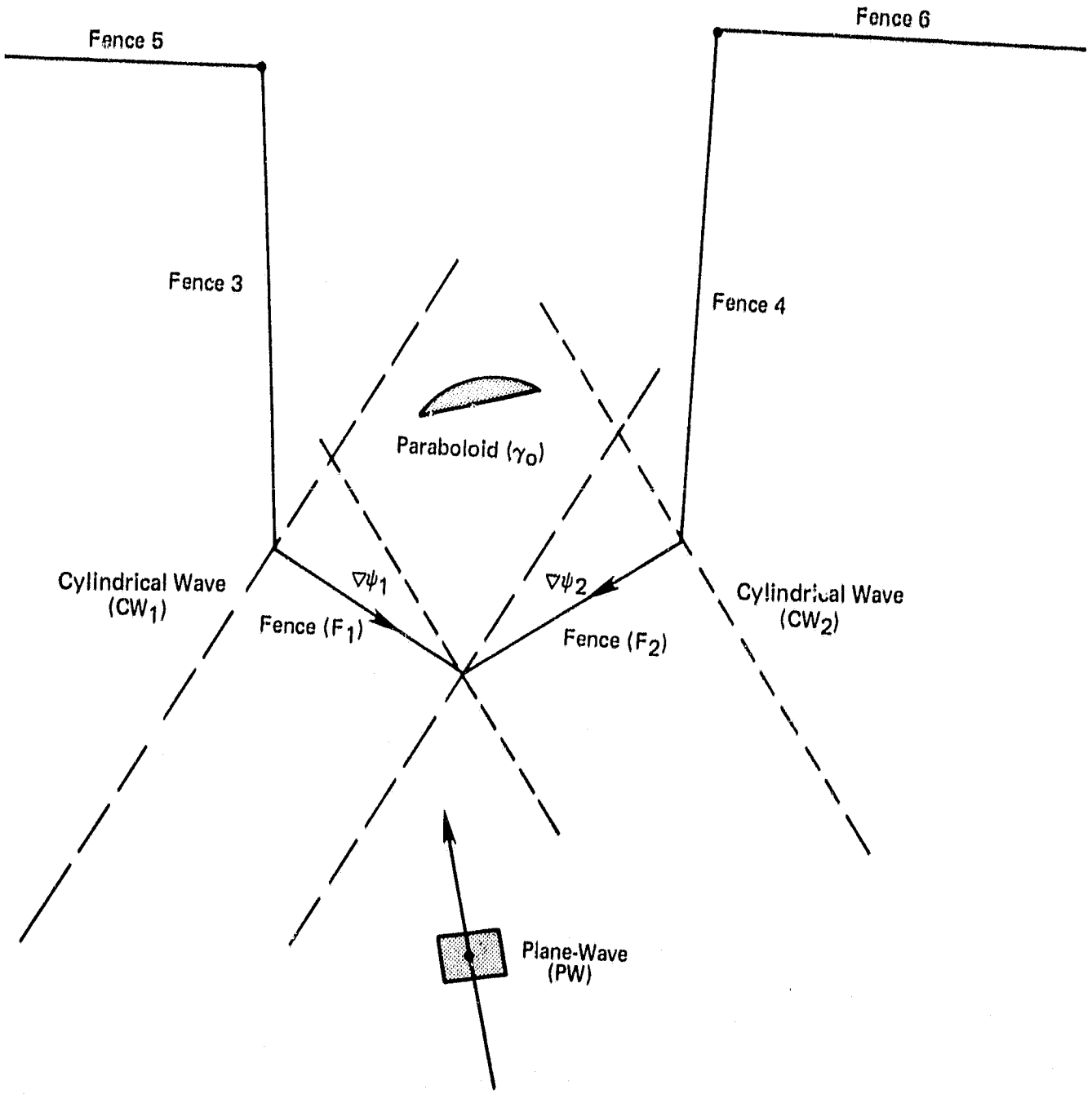

Figure 1. Illumination of Reflector (γ_o) due to Primary Source (PW) and Secondary Sources (CW_1) and (CW_2).

ORIGINAL PAGE IS
OF POOR QUALITY

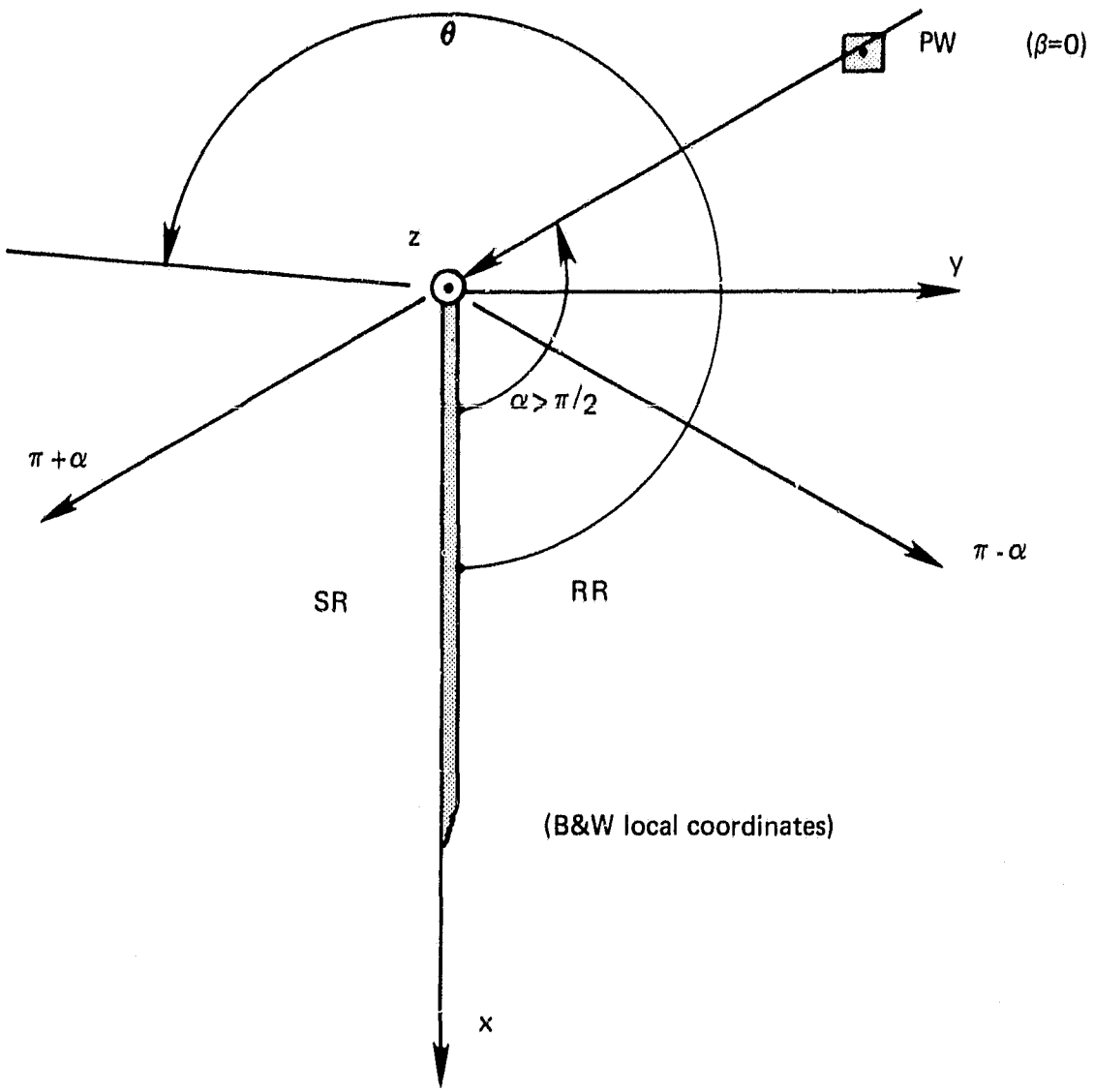

Figure 2. The Shadow and Reflection Regions (SR, RR) for $\alpha > \pi/2$, $\beta = 0$.

ORIGINAL PAGE IS
OF POOR QUALITY

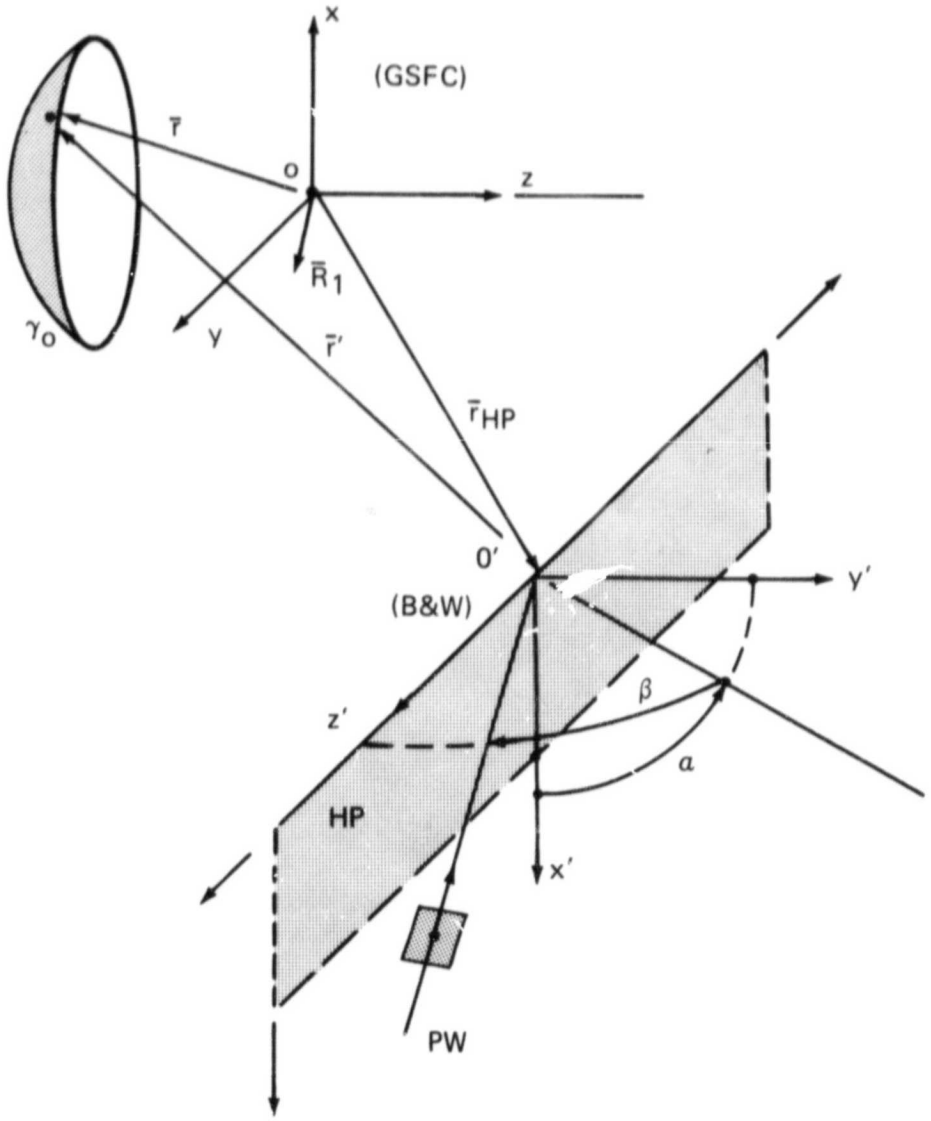

Figure 3. Coordinate Systems before Rotation of Half-Plane

ORIGINAL PAGE IS
OF POOR QUALITY

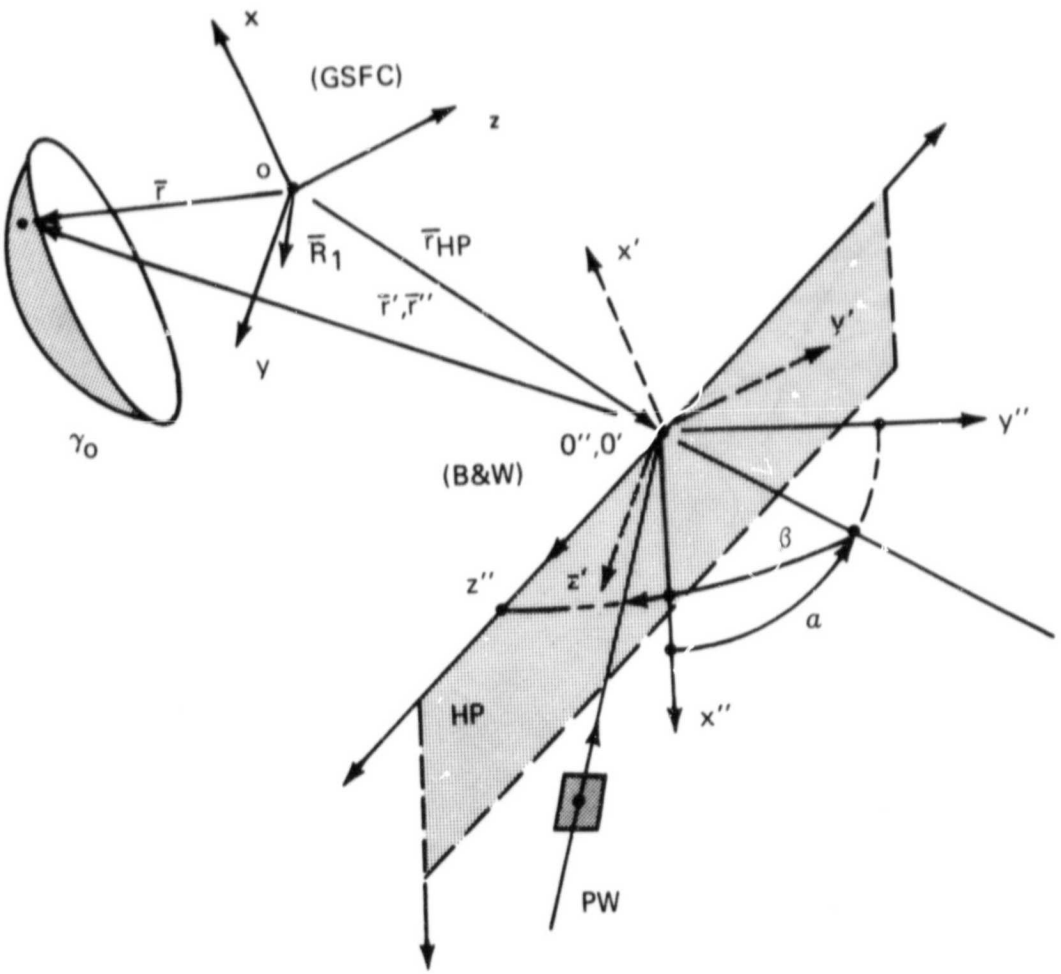

Figure 4. Coordinate Systems after Rotation of Half-Plane

ORIGINAL PAGE IS
OF POOR QUALITY

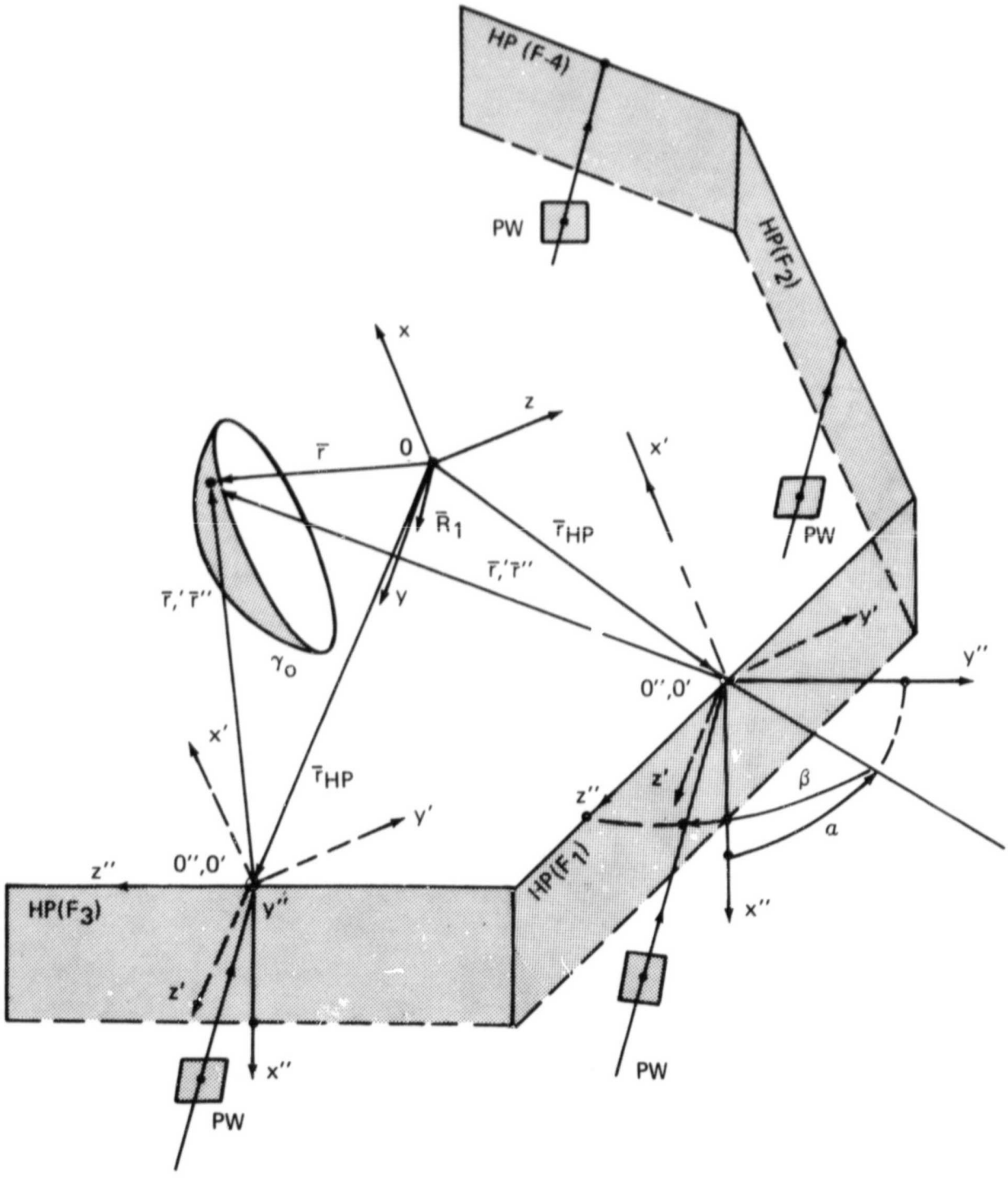

Figure 5. Coordinate Sys ems after Rotation of Half-Planes (Fixed Plane-Wave Source)

ORIGINAL PAGE IS
OF POOR QUALITY

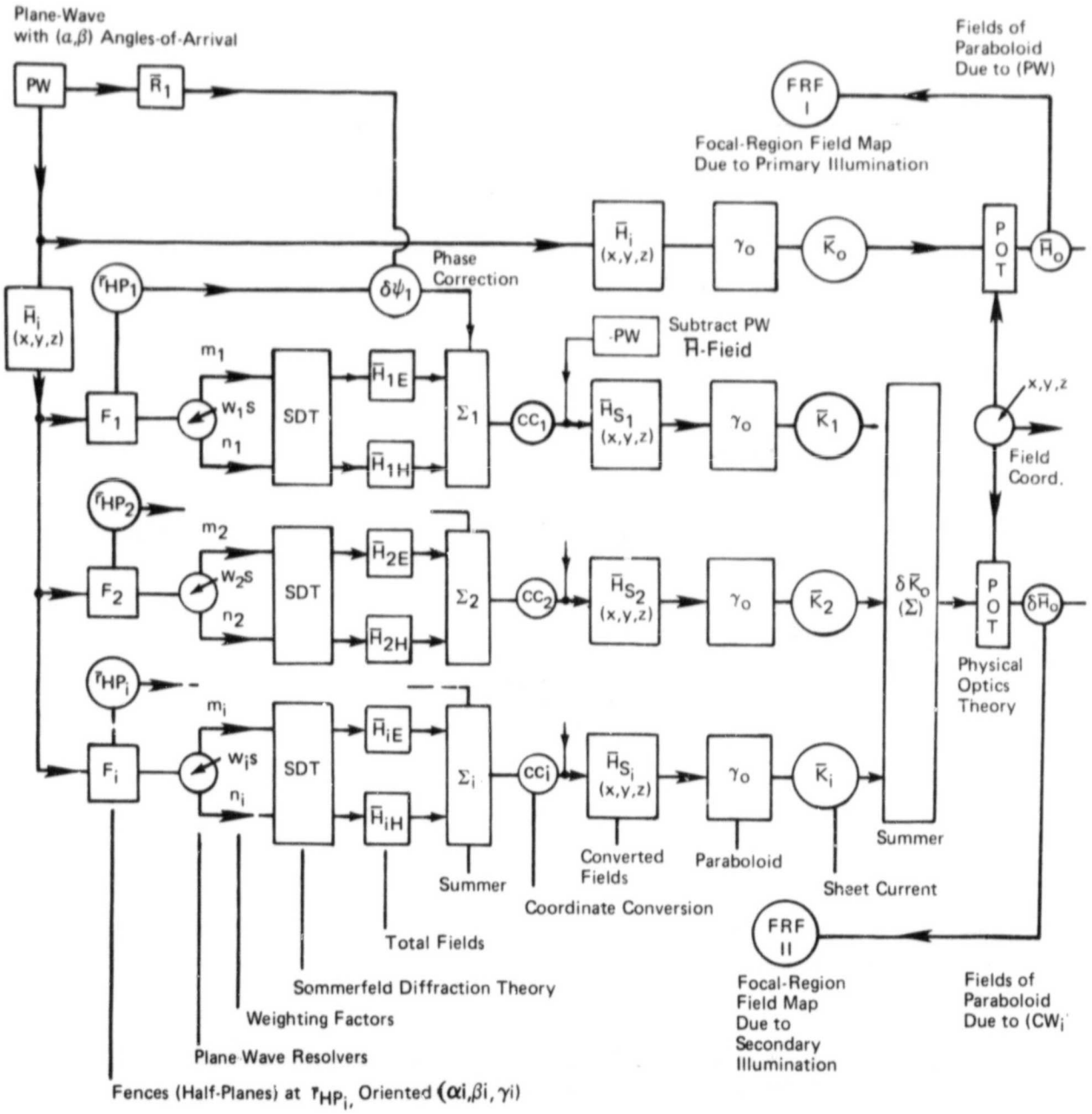

Figure 6. Flow-Chart Showing Computation of Focal-Region Fields (FRF I) and Perturbation (FRF II).

ORIGINAL PAGE IS
OF POOR QUALITY

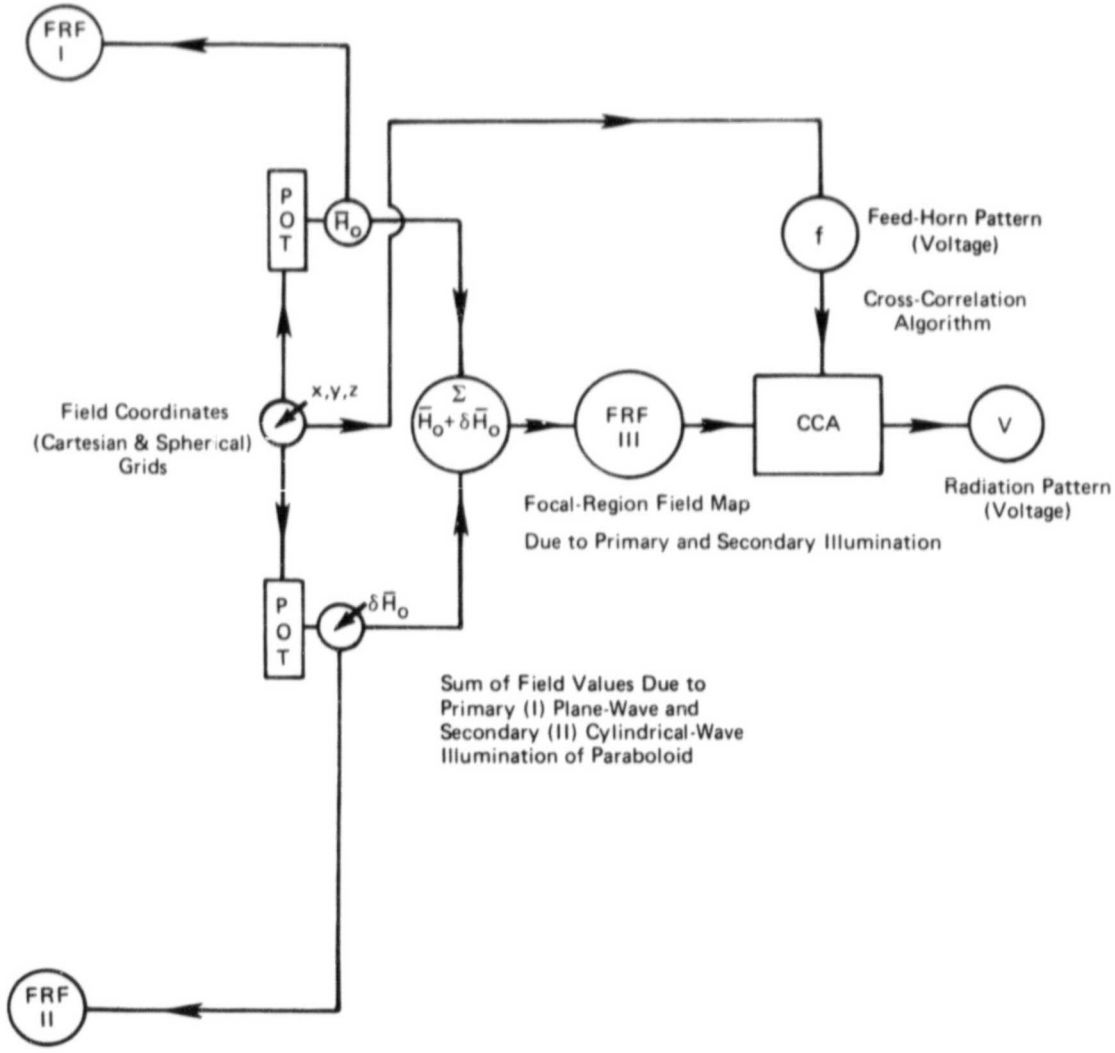

Figure 7. Flow-Chart Showing Computation of Combined Focal-Region Fields (FRF III) and Radiation Pattern

ORIGINAL PAGE IS
OF POOR QUALITY

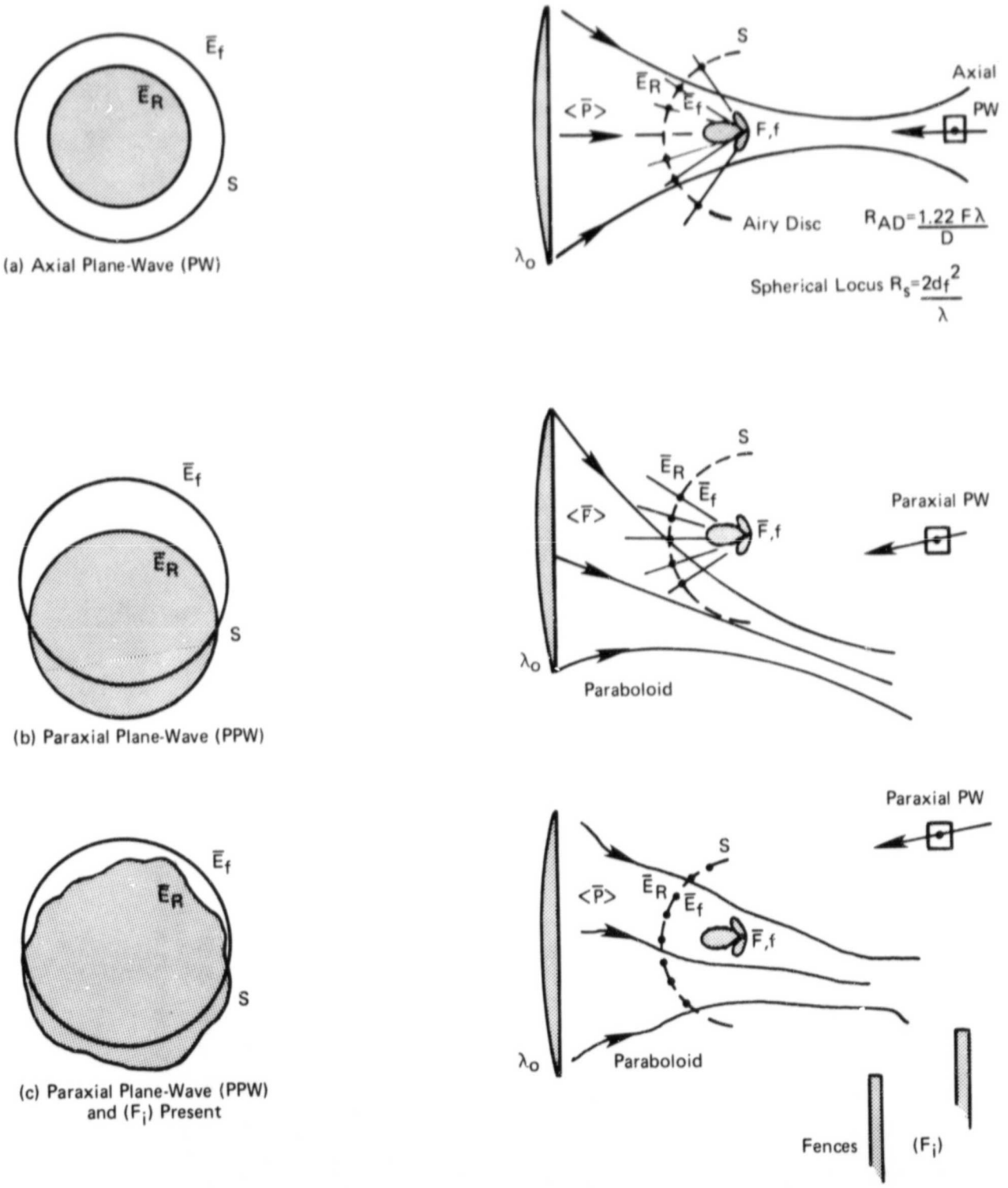

Figure 8. Cross-Correlation of Feed-Pattern ($\bar{E}_f$) and Received-Field ($\bar{E}_R$) on Spherical Locus (S)

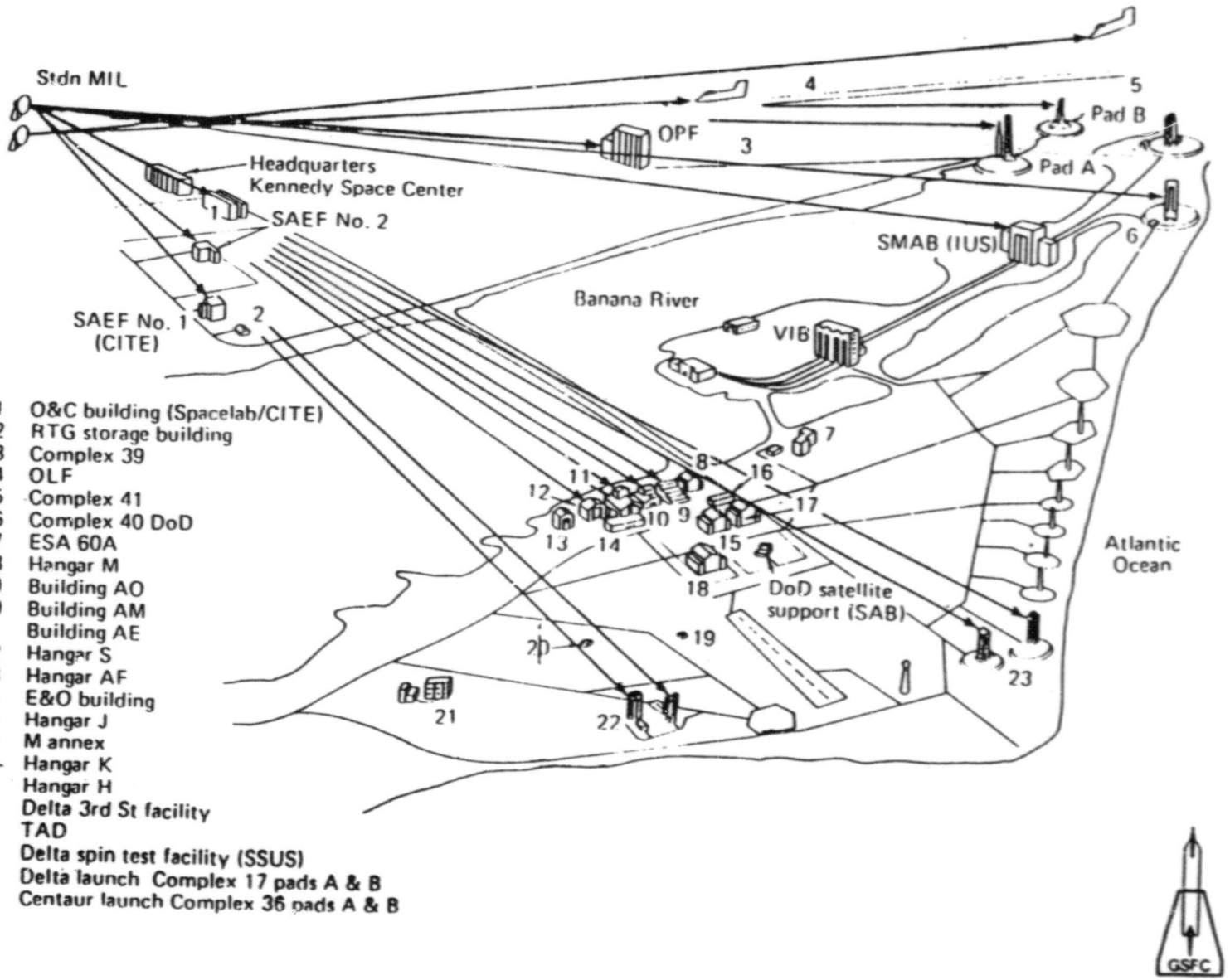

Figure 9. Kennedy Space Center Layout (KSC)

ORIGINAL PAGE IS
OF POOR QUALITY

ORIGINAL PAGE IS
OF POOR QUALITY

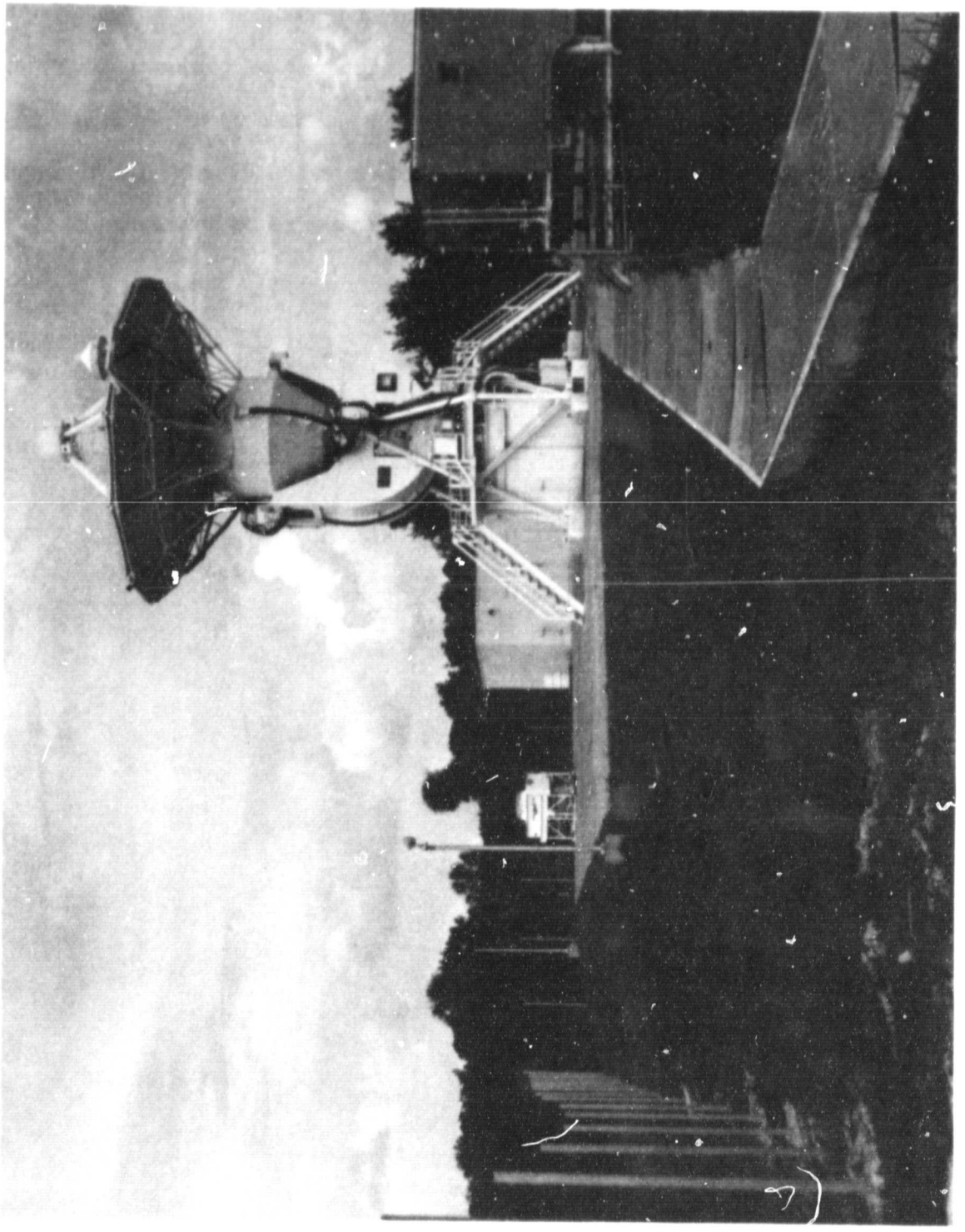

Figure 10. 30-Foot (9-M) USB Antenna No. 2

ACKNOWLEDGMENTS

This document is based on several classical electromagnetic developments, particularly those of Kirchhoff and Sommerfeld. Other standard procedures pertaining to rotation, polarization, and cross-correlation were appropriated from the literature as indicated by the list of references. The author is particularly indebted to R. Meneghini of the Goddard Laboratory for Atmospheric Sciences for guidance regarding the derivation of the H-plane polarization formulation and an analysis of Fresnel integrals.

REFERENCES

1. Born, M. and Wolf, E., "Principles of Optics," 2nd Edition, Pergamon Press, 1964.
2. Stratton, J. A., "Electromagnetic Theory," McGraw-Hill Book Company, Inc., 1941.
3. Silver, S., "Microwave Antenna Theory and Design," McGraw-Hill Book Company, Inc., 1949.
4. Schmidt, R. F., "The Calculation of Electromagnetic Fields by the Kirchhoff-Kottler Method," GSFC-X-525-70-293, May 1970.
5. Schmidt, R. F., "The Calculation of Electromagnetic Fields in the Fresnel and Fraunhofer Regions using Numerical Integration Methods," GSFC-X-811-71-392, July 1971.
6. Goldstein, H., "Classical Mechanics," Addison-Wesley Publishing Company, Inc., 1959.
7. Apostol, T. M., "Mathematical Analysis," Addison-Wesley Publishing Company, Inc., 1960.
8. Collin, R. E. and Zucker, F. J., "Antenna Theory," McGraw-Hill Book Company, Inc., 1969.
9. Beckmann, P., "The Depolarization of Electromagnetic Waves," The Golem Press, 1968.
10. Kaplan, W., "Advanced Calculus," Addison-Wesley Publishing Company, Inc., 1959.
11. Jackson, J. D., "Classical Electrodynamics," John Wiley and Sons, Inc., 1962.

ORIGINAL PAGE IS
OF POOR QUALITY

APPENDIX A

Scattered Fields for H-plane Polarization

The evaluation of equations (20) and (21) requires the partial derivatives (U_x) and (U_y) for the H-plane polarization case. An expression for (U), given in Ref. 1, p. 580, may be used to form (U_x) and (U_y) for the E-plane polarization case only, and these partial derivatives may be verified by utilization in equations (18) and (19) to obtain the explicit field equations (12) through (17). This process is now carried out in detail. Subsequently an expression for (U) of the H-plane polarization case is found and the process is repeated so that explicit field equations may be written.

E-plane Polarization:

$$U = \frac{e^{-\pi/4}}{\sqrt{\pi}} \sec\beta e^{ik(r\cos\beta - z\sin\beta)} [G(p) - G(q)] = Ce^{ikr\cos\beta} [G(p) - G(q)] = Ce^{iE} [G(p) - G(q)] \quad (1\text{-A})$$

Here $C = e^{-\pi i/4} \sec\beta/\sqrt{\pi}$, and $E = ik\cos\beta$.

$$p = -(2kr\cos\beta)^{1/2} \cos\frac{1}{2}(\theta - \alpha) \quad , \quad q = -(2kr\cos\beta)^{1/2} \cos\frac{1}{2}(\theta + \alpha) \quad (2\text{-A})$$

$$x = r\cos\theta \quad , \quad y = r\sin\theta \quad (3\text{-A})$$

$$-ip^2 = -ik\cos\beta(r + x\cos\alpha + y\sin\alpha) = -i(E + A) \quad (4\text{-A})$$

where $A = k\cos\beta(x\cos\alpha + y\sin\alpha)$

$$-iq^2 = -ik\cos\beta(r + x\cos\alpha - y\sin\alpha) = -i(E + B) \quad (5\text{-A})$$

where $B = k\cos\beta(x\cos\alpha - y\sin\alpha)$

$$G(p) = e^{-ip^2} \int_p^\infty e^{i\mu^2}\, d\mu \quad , \quad G(q) = e^{-iq^2} \int_q^\infty e^{i\mu^2}\, d\mu \quad (6\text{-A})$$

$$U = Ce^{-iA} \int_p^\infty e^{i\mu^2}\, d\mu - Ce^{-iB} \int_q^\infty e^{i\mu^2}\, d\mu \quad (7\text{-A})$$

$$U_x = Ce^{-iA} \frac{\partial}{\partial x} \int_p^\infty e^{i\mu^2}\, d\mu - Ce^{-iB} \frac{\partial}{\partial x} \int_q^\infty e^{i\mu^2}\, d\mu + C \frac{\partial e^{-iA}}{\partial x} \int_p^\infty e^{i\mu^2} d\mu - C \frac{\partial e^{-iB}}{\partial x} \int_q^\infty e^{i\mu^2} d\mu \quad (8\text{-A})$$

ORIGINAL PAGE IS
OF POOR QUALITY

Applying Leibnitz's Rule to equation (8-A),

$$U_x = -Ce^{-iA}\, e^{i(E+A)}\, \frac{\partial p}{\partial x} + Ce^{-iB}\, e^{i(E+B)}\, \frac{\partial q}{\partial x} - Cik\, \cos\beta\, \cos\alpha \left(e^{-iA} \int_p^\infty e^{i\mu^2}\, d\mu - e^{-iB} \int_q^\infty e^{i\mu^2}\, d\mu \right) \tag{9-A}$$

After simplification,

$$U_x = -Ce^{iE} \left\{ ik\, \cos\beta\, \cos\alpha\, [G(p) - G(q)] + \frac{\partial}{\partial x}\, (p - q) \right\} , \tag{10-A}$$

where

$$p - q = \frac{-2}{\sqrt{2}} (2\, k\, \cos\beta)^{1/2}\, \sin\frac{\alpha}{2}\, [\, (x^2 + y^2)^{1/2} - x\,]^{1/2} \tag{11-A}$$

and

$$\frac{\partial(p - q)}{\partial x} = \frac{(2\, k\, \cos\beta)^{1/2}}{\sqrt{r}}\, \sin\frac{\alpha}{2}\, \sin\frac{\theta}{2} . \tag{12-A}$$

Substituting (12-A) into (10-A), and using

$$H_y = \frac{i}{k}\, U_x , \tag{19}$$

equation (16) is verified.

A similar process produces

$$U_y = -Ce^{iE} \left\{ ik\, \cos\beta\, \sin\alpha\, [G(p) + G(q)] + \frac{\partial}{\partial y}\, (p - q) \right\} \tag{13-A}$$

and

$$\frac{\partial(p - q)}{\partial y} = -\left(\frac{\cos\, \theta/2}{\sin\, \theta/2} \right) \frac{\partial(p - q)}{\partial x} . \tag{14-A}$$

Substituting (14-A) into (13-A), and using

$$H_x = -\frac{i}{k}\, U_y , \tag{19}$$

equation (15) is verified.

An expression for (U), appropriate for the H-plane polarization case may be forced directly from a specialized case ($\beta \equiv 0$) in Ref. 1, p. 574. Using (21) of the present document,

ORIGINAL PAGE IS
OF POOR QUALITY

$$U = \frac{e^{-\pi i/4}}{\sqrt{\pi}} \sec\beta \, e^{ik(r\cos\beta - z\sin\beta)} [G(p) + G(q)] = Ce^{ik\, r\cos\beta} [G(p) + G(q)] = Ce^{iE} [G(p) + G(q)] \quad (15\text{-A})$$

Using equations (2-A) through (6-A),

$$U = Ce^{-iA} \int_p^\infty e^{i\mu^2} \, d\mu + Ce^{-iB} \int_q^\infty e^{i\mu^2} \, d\mu \quad (16\text{-A})$$

$$U_x = Ce^{-iA} \frac{\partial}{\partial x} \int_p^\infty e^{i\mu^2} \, d\mu + Ce^{-iB} \frac{\partial}{\partial x} \int_q^\infty e^{i\mu^2} \, d\mu + C \frac{\partial}{\partial x} e^{-iA} \int_p^\infty e^{i\mu^2} \, d\mu +$$

$$C \frac{\partial}{\partial x} e^{-iB} \int_q^\infty e^{i\mu^2} \, d\mu \quad . \quad (17\text{-A})$$

Using Leibnitz's Rule,

$$U_x = -Ce^{-iA} e^{i(E+A)} \frac{\partial p}{\partial x} - Ce^{-iB} e^{i(E+B)} \frac{\partial q}{\partial x}$$

$$- Cik \cos\beta \cos\alpha \left(e^{-iA} \int_p^\infty e^{i\mu^2} \, d\mu + e^{-iB} \int_q^\infty e^{i\mu^2} \, d\mu \right) \quad . \quad (18\text{-A})$$

After simplification,

$$U_x = - Ce^{iE} \left\{ ik \cos\beta \cos\alpha \, [G(p) + G(q)] + \frac{\partial}{\partial x} (p + q) \right\} \quad (19\text{-A})$$

where

$$p + q = -\frac{2}{\sqrt{2}} (2k \cos\beta)^{1/2} \cos \frac{\alpha}{2} \, [(x^2 + y^2)^{1/2} - x]^{1/2} \quad (20\text{-A})$$

and

$$\frac{\partial}{\partial x} (p + q) = - \frac{(2k \cos\beta)^{1/2}}{\sqrt{r}} \cos \frac{\alpha}{2} \cos \frac{\theta}{2} \quad . \quad (21\text{-A})$$

Substituting (21-A) into (19-A), and using

$$E_y = - \frac{i}{k} \frac{\partial U}{\partial x} \quad , \quad (21)$$

ORIGINAL PAGE IS
OF POOR QUALITY

equation (23) is obtained.

A similar process produces

$$U_y = -Ce^{iE}\left\{ik\cos\beta\sin\alpha[G(p) - G(q)] + \frac{\partial}{\partial y}(p + q)\right\} \qquad (22\text{-A})$$

and

$$\frac{\partial}{\partial y}(p + q) = -\frac{(2k\cos\beta)^{1/2}}{\sqrt{r}}\cos\frac{\alpha}{2}\sin\frac{\theta}{2} \quad , \qquad (23\text{-A})$$

Substituting (23-A) into (22-A), and using

$$E_x = \frac{i}{k}\frac{\partial U}{\partial y} \quad , \qquad (20)$$

equation (22) is obtained.

Returning to equations (20) and (21), (24) through (27) are obtained immediately using (U), (U_x), and (U_y). Equations (22), (23), and (27) should be compared to those of the specialized case (β=0) of Ref. 1, p. 574.

APPENDIX B

ORIGINAL PAGE IS
OF POOR QUALITY

The Fresnel Integrals

$a > 0$:

$$F(a) = \int_a^\infty e^{i\mu^2}\, d\mu \tag{1-B}$$

$a < 0$:

$$F(a) = \int_{-|a|}^\infty e^{i\mu^2}\, d\mu = \int_{-|a|}^0 e^{i\mu^2}\, d\mu + \int_0^\infty e^{i\mu^2}\, d\mu \tag{2-B}$$

Let $\mu \to -\mu$ so that

$$\int_{\mu_1 = -|a|}^{\mu_2 = 0} e^{i\mu^2}\, d\mu = \int_{\mu_1 = |a|}^{\mu_2 = 0} e^{i\mu^2}\, d\mu = \int_0^{|a|} e^{i\mu^2}\, d\mu \tag{3-B}$$

$a < 0$:

$$F(a) = 2\int_0^\infty e^{i\mu^2}\, d\mu - \int_{|a|}^\infty e^{i\mu^2}\, d\mu \tag{4-B}$$

using (2-B), (3-B) and

$$\int_0^{|a|} e^{i\mu^2}\, d\mu = \int_0^\infty e^{i\mu^2}\, d\mu - \int_{|a|}^\infty e^{i\mu^2}\, d\mu \tag{5-B}$$

From Ref. 1, p. 573, equation (35),

$$G(0) = \int_0^\infty e^{i\mu^2}\, d\mu = \frac{1}{2}\sqrt{\pi}\, e^{\pi i/4} \tag{6-B}$$

so that

$$G(a) = e^{-ia^2}\left[\sqrt{\pi}\, e^{\pi i/4}\, U(-a) + \mathrm{sgn}(a)\int_{|a|}^\infty e^{i\mu^2}\, d\mu\right] \tag{7-B}$$

for

$$U(x) \equiv 1 \mid x > 0 \qquad 0 \mid x \leq 0 \tag{8-B}$$

and

ORIGINAL PAGE IS
OF POOR QUALITY

$$\text{sgn}(x) = +1 \mid x \geq 0 \qquad -1 \mid x < 0 \tag{9-B}$$

is a general formula for (a) positive, negative, or zero.

For G(a) to be continuous at a = 0,

$$\lim_{\epsilon \to 0} G(-\epsilon) = \lim_{\epsilon \to 0} G(\epsilon) = G(0) = \frac{\sqrt{\pi}}{2} e^{\pi i/4} \tag{10-B}$$

See Ref. 1, p. 76.

$$G(-\epsilon) = e^{-i\epsilon^2} \left[\sqrt{\pi}\, e^{\pi i/4} - \int_{|\epsilon|}^{\infty} e^{i\mu^2}\, d\mu\right] \tag{11-B}$$

$$G(\epsilon) = e^{-i\epsilon^2} \int_{|\epsilon|}^{\infty} e^{i\mu^2}\, d\mu \tag{12-B}$$

$$\lim_{|\epsilon| \to 0} \int_{|\epsilon|}^{\infty} e^{i\mu^2}\, d\mu = \frac{\sqrt{\pi}}{2} e^{\pi i/4} \tag{13-B}$$

therefore (10-B) is satisfied.

Using

$$e^{-ia^2} \int_{|a|}^{\infty} e^{i\mu^2}\, d\mu = \frac{i}{2|a|} + 0\left(\frac{1}{|a|^3}\right) \tag{14-B}$$

when (a) is large,

$$G(a) = \sqrt{\pi}\, e^{\pi i/4}\, e^{-ia^2}\, U(-a) + \text{sgn}(a) \frac{i}{2|a|} + 0\left(\frac{1}{|a|^3}\right) \tag{15-B}$$

See Ref. 1, p. 572, equations (29) and (30) for the origin of equation (14-B).

ORIGINAL PAGE IS
OF POOR QUALITY

APPENDIX C

Units and Dimensions

The Kirchhoff-Kottler (physical-optics) formulation of equations (8) through (11) of this document is in the rationalized MKS system of units. It is characteristic of this system of units that, in the far-field, the ratio of the magnitude of the electric to the magnetic field yields the free-space impedance (Z_o). This is easily seen from

$$\frac{|\bar{E}|\,(V/m)}{|\bar{H}|\,(AT/m)} = \frac{\left|-j\omega\mu_o \frac{1}{4\pi}\int_{S_1}(\bar{n}\times\bar{H}_1)\,\psi\,dS\right|}{\left|-\frac{1}{4\pi}\int_{S_1}(\bar{n}\times\bar{H}_1)\times\nabla\psi\,dS\right|} = \frac{\omega\mu_o}{k} = \sqrt{\frac{\mu_o}{\epsilon_o}} = Z_o\ (\text{ohms}) \tag{1-C}$$

using (8) and (9) as $r \to \infty$.

The plane wave formulation, (1) through (4) and the solution for the half-plane, (12) through (17) and (22) through (27), as obtained from Ref. 1 is in Gaussian units. Conversion of units may be formally effected using Ref. 11. In view of the fact that the magnetic fields are of prime interest throughout this paper it is convenient to multiply all electric fields of Ref. 1 by a numerical factor

$$F_N = (Z_o)_N = \left(\sqrt{\frac{\mu_o}{\epsilon_o}}\right)_N = 377\ , \tag{2-C}$$

Suppressing the units ohms for (F_N). The electric field and magnetic field expressions obtained from Ref. 1 may then be taken as volts/meter (V/m) and ampere-turns (AT/m), respectively. In the far-field

$$\frac{|\bar{E}_{FF}|}{|\bar{H}_{FF}|} = F_N \frac{|\bar{E}_{V/m}|}{|\bar{H}_{AT/m}|} = Z_o \text{ ohms} \quad . \tag{3-C}$$

APPENDIX D

ORIGINAL PAGE IS
OF POOR QUALITY

The Total Field

Equations (12) through (17) and (22) through (27) represent the total fields associated with a given half-plane. This may be seen by considering the special case ($\beta = 0$) and the electric field in the reflection region ($p < 0$, $q < 0$), the illuminated region ($p < 0$, $q > 0$), and the shadow region ($p > 0$, $q > 0$), respectively, for a remote observer ($r \to \infty$). The G(p) and G(q) of the field equations, cited above, then lead to the indentification of interfering incident and reflected plane waves, a transmitted or incident plane wave, and the degenerate or zero plane wave for the regions named upon application of half-angle identity formulas. Collectively these constitute the geometric optics field for the special case being considered:

$$E_z^{(g)} = \begin{cases} e^{-ikr\cos(\theta-\alpha)} - e^{-ikr\cos(\theta+\alpha)}, & 0 \leqslant \theta < \pi - \alpha \\ e^{-ikr\cos(\theta-\alpha)}, & \pi - \alpha < \theta < \pi + \alpha \\ 0, & \pi + \alpha < \theta \leqslant 2\pi \end{cases} \qquad (1\text{-D})$$

See Ref. 1, p. 572, eqn. (33).

From the preceding it follows that the geometric optics field is contained in the field solution of each half-plane ($\beta \neq 0$ in general), for electric and magnetic fields, and must be subtracted (i) times when (i) fences are considered in the present simulation. The paraboloid is illuminated directly by a specified incident plane-wave, and will not lie in either the shadow or reflection regions.